Finite element analysis and experimental study on the sealing performance of low-phenyl silicone rubber sealing rings

Received 18 November 2024
Revised 9 December 2024
Accepted 11 December 2024

Ming Gao
Metals and Chemistry Research Institute, China Academy of Railway Sciences Corporation Limited, Beijing, China
Dongkai Li and Kun Liu
Department of Locomotive and Car, China State Railway Group Company Limited, Beijing, China
Shuliang Xu and Feng Zhao
Rolling Stock Department, China Railway Harbin Group Company Limited, Harbin, China, and
Ben Guo, Anhui Pan, Xiao Xie and Huanre Han
Metals and Chemistry Research Institute, China Academy of Railway Sciences Corporation Limited, Beijing, China

Abstract

Purpose – The brake pipe system was an essential braking component of the railway freight trains, but the existing E-type sealing rings had problems such as insufficient low-temperature resistance, poor heat stability and short service life. To address these issues, low-phenyl silicone rubber was prepared and tested, and the finite element analysis and experimental studies on the sealing performance of its sealing rings were carried out.

Design/methodology/approach – The low-temperature resistance and thermal stability of the prepared low-phenyl silicone rubber were studied using low-temperature tensile testing, differential scanning calorimetry, dynamic thermomechanical analysis and thermogravimetric analysis. The sealing performance of the low-phenyl silicone rubber sealing ring was studied by using finite element analysis software abaqus and experiments.

Findings – The prepared low-phenyl silicone rubber sealing ring possessed excellent low-temperature resistance and thermal stability. According to the finite element analysis results, the finish of the flange sealing surface and groove outer edge should be ensured, and extrusion damage should be avoided. The sealing rings were more susceptible to damage in high compression ratio and/or low-temperature environments. When the sealing effect was ensured, a small compression ratio should be selected, and rubbers with hardness and elasticity less affected by temperature should be selected. The prepared low-phenyl silicone rubber sealing ring had zero leakage at both room temperature (RT) and −50 °C.

Originality/value – The innovation of this study is that it provides valuable data and experience for the future development of the sealing rings used in the brake pipe flange joints of the railway freight cars in China.

Keywords Low-phenyl silicone rubber, Sealing ring, Sealing performance, Finite element analysis, Leakage

Paper type Research paper

This work is supported by the Science and Technology Research and Development Plan of the China State Railway Group Company Limited (No. Q2023J012).

Railway Sciences
Vol. 4 No. 1, 2025
pp. 123-137
Emerald Publishing Limited
e-ISSN: 2755-0915
p-ISSN: 2755-0907
DOI 10.1108/RS-11-2024-0047

1. Introduction

Brake pipe systems are essential components of braking systems in railway freight car. Flange joints and sealing rings are commonly used for connection and sealing, with the sealing performance of the sealing ring directly affecting the safety of the train operation (Lv, Yi, Zhu, Chen, & Li, 2009; Liu, Yang, Chen, Zhang, & Zhou, 2023). During train movement, if leakage of the sealing ring occurs, pressure cannot be held during braking. Then, brake malfunctions or the air pressure of the train will not reach the specified pressure, potentially causing the train to stop midway (Cheng *et al.*, 2022; Fu, 2022; Gao *et al.*, 2024). Furthermore, due to the lack of professional vehicle maintenance personnel on the train, issues affecting train operation time and traffic order cannot be resolved quickly, which will cause train delays and pose a threat to safe train operation. In case of severe winter in northern China, leakage of brake pipe systems occurs more frequently, severely affecting safe train operation.

Leakage of the sealing ring in brake pipe systems refers to compressed air flowing from inside to the outside of pipe systems, including interface, destruction, penetration, and diffusion leakage, with interface leakage and destruction leakage predominant (Akhtar, Qamar, Pervez, & Al-Jahwari, 2018; Cheng *et al.*, 2022; Hu, Zhang, & Chen, 2020). Interface leakage occurs when compressed air escapes through the interface between internal and external environments (the sealing surface). This type of leakage is primarily caused by gaps at the interface, driven by the pressure difference between the two sides of the contact surfaces. Destruction leakage results from damage to the sealing component caused by external forces exceeding the fatigue strength or material aging and deterioration, thus, producing leakage. Several factors affect the sealing performance of sealing rings, including the hardness of the rubber (duration of use, ambient temperature), the working conditions (medium pressure), compression stress, and the roughness of the joint sealing surface. After using for a certain period of time, the sealing rings will experience aging, the hardness of the rubber will increase, and the sealing performance will decline. Besides, under low-temperature conditions, the rubber will become harder and less elastic, causing the sealing surface gap to widen and increasing the occurrence of leakage. Especially in cold regions of northern China, some train cars frequently move in and out of high-temperature thawing warehouses, accelerating rubber aging. In summary, the primary factors affecting the sealing surface performance are the sealing properties of the sealing rubber rings and the ambient temperature. Common types of rubber for sealing rings include nitrile rubber, silicone rubber, and fluorosilicone rubber, among which silicone rubber possesses excellent low-temperature resistance and thermal stability.

Silicone rubber has good high- and low-temperature resistance and processing performance, while fluorosilicone rubber also has good high and low temperature resistance and excellent oil resistance, but the price of fluorosilicone rubber is too expensive. (Song, Yang, Wang, & Su, 2024) Silicone rubber is a linear macromolecular polymer with silicon-oxygen bonds comprising the main chain and monovalent organic groups as the side chains, endowing the polymer with excellent thermal stability. In phenyl silicone rubber, a certain proportion of diphenylsiloxane chain units or methylphenylsiloxane chain units can be introduced into methyl vinyl silicone rubber to improve low-temperature resistance, allowing the material to function long-term in a temperature range of −70 °C-250 °C (Akhlaghi *et al.*, 2017; Huang, Mu, & Su, 2021; Lou, Zhang, Jin, Liu, & Dai, 2018; Wang *et al.*, 2023, 2024). Low-phenyl silicone rubber exhibits the best low-temperature resistance and can effectively reduce the chance of sealing rings leakage at low temperatures. However, it has moderate tear resistance, which may lead to destruction leakage. Lee, Yoo, Kim, Kang, and Kim (2012), Wang, Ren, Liu, Hao, and Yang (2013) numerous studies have examined the low-temperature properties of low-phenyl silicon rubber, however, there remains a lack of research on the sealing performance and finite element analysis of sealing rings. Therefore, in this work, we explored the changes in the mechanical properties and dynamic features of low-phenyl silicone rubber at room temperature (RT) and low temperature (−50 °C). We also used finite element analysis and experiments to investigate

the sealing performance of low-phenyl silicone rubber sealing rings, to aid in the design and application of resistant silicone rubber sealing rings at high- and low-temperature.

2. Experimental section

2.1 Materials

The following materials were used: L-120 low-phenyl silicone rubber (phenyl molar fraction 5% and vinyl molar fraction 0.2%, Guangzhou Laysou Chemical Technology Co., Ltd.), fumed silica (A380, Evonik Industries AG., Germany), and 2,5-dimethyl-2, 5-di (tert-butylperoxy) hexane (Dow Chemical Company, USA). All reagents were commercially available.

2.2 Instruments and equipment

The following instruments and equipment were used: an internal mixer (ML-1.5, Baihong Machinery (Shanghai) Co., Ltd.), an open mixing mill (XK-160, Dalian Yunshan Machinery Co., Ltd.), a flat vulcanizing machine (XLB-D 400 × 400, Zhejiang Huzhou Dongfang Machinery Co., Ltd.), a universal testing machine (Zwick Z020, Zwick Roell Group, Germany), a hardness tester (digitest II, Bareiss Prüfgerätebau GmbH, Germany), a low-temperature brittleness tester (single experiment method) (GT-7006-VR, Gotech Testing Machines, Inc.), a compression cold resistance coefficient tester (GT-7006-VR, Gotech Testing Machines, Inc.), a dynamic thermomechanical analyzer (DMA1, Mettler Toledo, USA), a differential scanning calorimeter (DSC 204 F1, NETZSCH Group, Germany), and a thermogravimetric analyzer (TG 209 F3, NETZSCH Group, Germany).

2.3 Preparation of the test samples

The basic recipe consisted of 100 parts of low-phenyl silicone rubber, 45 parts fumed silica, 5 parts structure control agent, and 0.5 parts vulcanizing agent.

First, the raw rubber was plasticized in an open mixing mill. After roll banding, 1/3 of the fumed silica and structure control agent was added. After even mixing, another 1/3 of the fumed silica and structure control agent was added, and after additional mixing, the remaining fumed silica and structure control agent was added. After the rubber was subjected to five milling cycles, the vulcanizing agent was added and the sample passed through five additional milling cycles to obtain a rubber sheet for future use.

The primary vulcanization condition of the rubber mix was 170 °C for 10 min, and the gauge pressure of the vulcanizing machine was 10 MPa. Secondary vulcanization was carried out in an electric heated blast oven at 200 °C for 4 h.

2.4 Measurements

The sample hardness was measured according to the GB/T 531–2008 hardness, while the tensile strength and elongation at break were measured following the GB/T 528–2009 standard, and the tear strength was measured according to GB/T 529–2008 standard. The compression cold resistance coefficient was determined according to the HG/T 3866–2008 standard, and the brittle temperature was determined according to the GB/T 1682–2014 standard. Compression mode was used during dynamic thermomechanical analysis (DMA), where the diameter and height of the cylindrical sample were both 9.5 mm. In addition, the heating range was −130 °C–150 °C, the heating rate was 5 °C/min, the frequency was 1 Hz, and the amplitude was 5 μm. Differential scanning calorimetry (DSC) was performed with a temperature range of −80 °C–25 °C, the heating rate was 10 °C/min, and measurements were conducted in a nitrogen atmosphere. For thermogravimetric analysis (TGA), the heating rate was 10 °C/min, the temperature range was 25 °C–800 °C, and measurement was performed under nitrogen flow. The sealing performance of the prepared low-phenyl silicone rubber

sealing ring was tested according to the Q/CR 706–2019 standard "E-shaped sealing ring for railway freight car brake pipe flange".

2.5 Construction of finite element analysis model of the sealing ring

Finite element analysis was conducted using large-scale finite element analysis software Abaqus. The finite element analysis model is shown in Figure 1, which consisted of a two-dimensional axisymmetric model using the DN32 specification sealing ring drawing with an inner diameter of 48 mm. For finite element calculation of the sealing ring, analysis included the entire assembly of the sealing ring, flange joints, and groove due to complex boundary conditions. Interactions between the sealing ring, flange joint, and groove resulted in a squeezing effect. Therefore, finite element analysis of the sealing ring involved the study of contact behavior between the rubber and metal materials. Due to the much higher elastic modulus of metal materials compared to rubber materials, flange joints and grooves were considered as rigid bodies in this paper.

2.5.1 Constitutive model of rubber material. Rubber materials are hyperelastic and almost incompressible bodies, with constitutive relations that are complex nonlinear functions typically represented by strain energy functions. When subjected to force, the rubber material will experience large displacement and large strain, with the mechanical model exhibiting complex material and geometric nonlinearity. The volume after deformation can be approximately considered unchanged, and as a result, its stress cannot be determined only by the deformation state, but also through a combination of deformation and medium pressure. The Ogden model is the most common expression of the constitutive model, and its strain energy density function W is expressed as follows:

$$W = \sum_{i=1}^{N} \frac{\mu_i}{\alpha_i}\left(\lambda_1^{\alpha_i} + \lambda_2^{\alpha_i} + \lambda_3^{\alpha_i} - 3\right) + \sum_{k=1}^{N} \frac{1}{D_k}(J-1)^{2k} \tag{1}$$

Among them, μ_i and α_i are material constants, the unit of μ_i is pressure unit, α_i has no dimension or unit, and the specific values of them are determined by the experiments. λ_1, λ_2, and λ_3 represent the principal elongation in three directions respectively. D_i is an incompressible parameter used to represent volume changes. N represents the order number of the model.

In this study, the Mises stress and contact stress of the low-phenyl silicone rubber sealing ring were simulated and analyzed using the third-order Ogden model. The model coefficients μ_i and α_i were fitted from the tensile test data of the low phenyl silicone rubber compound. Due to the fact that only uniaxial tensile test data were available in this paper, the rubber material

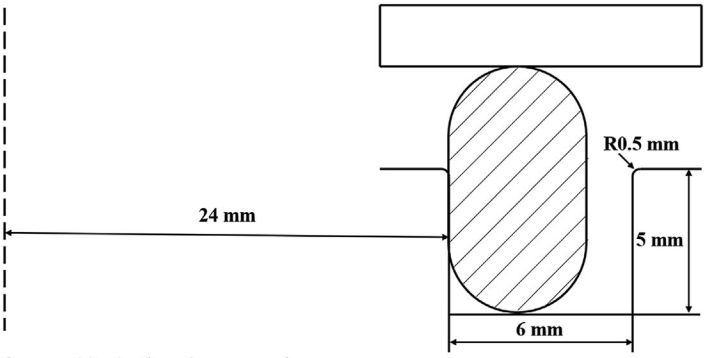

Source(s): Authors' own work

Figure 1. Schematic diagram of the finite element model of a sealing ring

was set as an incompressible material with $D_i = 0$, the second term on the right side of Equation (1) was ignored during fitting.

2.5.2 Boundary conditions of the finite element model of the sealing ring. Standard contact was set for the low-phenyl silicone rubber sealing ring and sealing groove, with the contact friction coefficient set to 0.5 (Cui, Qin, Di, & Yang, 2014; Jing, Mu, Zhou, & Xie, 2020; Li, Liu, Wang, & Leng, 2020). Finite analysis in this work included the following experimental conditions: (1) Two sealing modes. According to the sealing test requirements, this analysis was divided into flange joint zero-gap sealing (0 mm) and large gap assembly (1.8 mm). (2) Two experimental temperatures. The temperatures in this analysis included room temperature and −50 °C, based on the experimental results. (3) Different air pressures. Pressures of 0 and 0.6 MPa were applied inside the sealing ring to analyze its force variations with and without pressure.

The analysis of two sealing modes and two different inner air pressures were divided into two steps: (1) The deformation state of the sealing ring was first analyzed under no internal pressure. Then, the boundary points a and b of the sealing ring were extracted, which were respectively the inner boundary points between the sealing ring and the sealing surface of the flange body and the bottom surface of the sealing groove. (2) Applying an internal pressure of 0.6 MPa. The areas of the internal pressure application were located on the inside of the sealing ring bounded by the points a and b in the first step.

3. Results and discussion

3.1 Measurements of the properties of the low-phenyl silicone rubber

The thermal stability of silicone rubber endowed it with excellent heat aging resistance. In the low-phenyl silicone rubber, a bulky phenyl group was introduced into the molecular chain, destroying the regularity of the original structure, reducing the glass transition temperature of the silicone rubber, and allowing it to exhibit excellent low-temperature resistance (Huang *et al.*, 2021; Wang *et al.*, 2023, 2024). The measured physical properties of the low-phenyl silicone rubber material prepared in this study at room temperature and low temperature (−50 °C) are shown in Table 1. The results showed that the hardness, tensile strength, and tensile modulus of the specimen at low temperature (−50 °C) were slightly higher than at room temperature. Because the mobility of rubber segments declined at low temperatures, their hardness and strength increased. At low temperature (−50 °C), the hardness of the specimen

Table 1. Results of testing the properties of low-phenyl silicone rubber

No.	Test items		Test result
1	Hardness (Shore A)	Room temperature	60
2		Low temperature −50 °C	63
3	Tensile strength (MPa)	Room temperature	9.34
4		Low temperature −50 °C	9.63
5	Elongation at break	Room temperature	673%
6		Low temperature −50 °C	650%
7	Tear strength (right angle, kN/m)	Room temperature	21.7
8		Low temperature −50 °C	30.1
9	100% Tensile strength (MPa)	Room temperature	0.58
10		Low temperature −50 °C	0.59
11	300% Tensile strength (MPa)	Room temperature	2.04
12		Low temperature −50 °C	2.71
13	Compression cold resistance coefficient (−50 °C, Compression ratio 20%)		0.73
14	Brittle temperature		No damage at −60 °C

Source(s): Authors' own work

only increased from Shore A 60 to Shore A 63, and the 100% tensile modulus was generally consistent, while the 300% tensile modulus only increased by about 32.8%. The above results indicated the excellent low-temperature resistance of the prepared low-phenyl silicone rubber. The compression cold resistance coefficient of the low-phenyl silicone rubber was 0.73, with no damage in the brittle temperature test at −60 °C, also indicating the excellent low-temperature resistance of the prepared low-phenyl silicone rubber.

The molecular structure and properties of the rubber directly determined the sealing performance and service life of the sealing ring. In this work, low-temperature stretching, DSC, DMA, and TGA were employed to examine the low-temperature properties and thermal stability of the prepared low-phenyl silicone rubber.

The tensile stress-strain curves of the low-phenyl silicone rubber at room temperature and low temperature are shown in Figure 2 (a). All specimens exhibited distinct rubber elasticity characteristics, where the stress slowly increased at the beginning stage and rapidly increased in the late stage until specimen fractured (Nakanishi, Mita, Yamamoto, Ichino, & Takenaka, 2021; Tao, 2023). The mobility of the polymer material chain segments dropped in the low-temperature environments, which macroscopically resulted in increased modulus and hardness. When the strain was the same, the stress of the low-temperature specimen of the low-phenyl silicone rubber was only slightly higher than the room-temperature specimen, indicating the excellent low-temperature resistance of the low-phenyl silicone rubber. The fracture energy G_F was obtained by integrating the area under the stress-strain curve, and the values of the specimen at room temperature and low temperature (−50 °C) were 25.92 and 26.86 MJ/m^3, respectively (shown in Figure 2 (b)). At low temperatures, the mobility of the rubber chain segments decreased, and the strength increased. The low-phenyl silicone rubber exhibited excellent low-temperature resistance and small change in the strain under the same stress, while the calculated G_F at low temperatures increased.

Below the glass transition temperature (Tg), the rubber chain segments froze, and at this point, a hard and solid glassy state appeared. When the temperature increased to Tg, the chain segments started thawing. On the DSC heating curve, the shift of the baseline produced a step, the two baselines were extended in the opposite direction, and the temperature corresponding to their intersection was Tg (Wang *et al.*, 2023, 2024). Figure 3 presents the DSC heating curve of the prepared low-phenyl silicone rubber, where the measured Tg was −110 °C. After the stage of glass transition, the rubber entered into a high elastic state, no apparent crystallization and melting peaks were observed, and the sample belonged to non-crystalline rubber because the bulky phenyl group destroyed the regularity of the methyl vinyl silicone rubber. The above

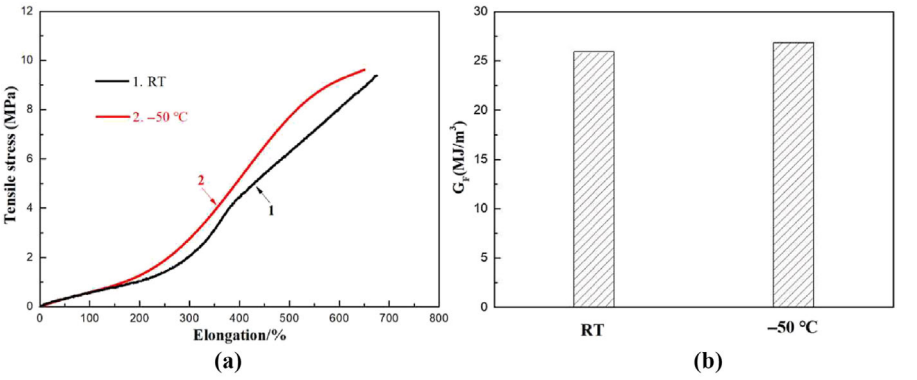

Source(s): Authors' own work

Figure 2. Tensile stress-strain curves (a) and fracture energy (b) of the low-phenyl silicone rubber at room temperature and low temperature (−50 °C)

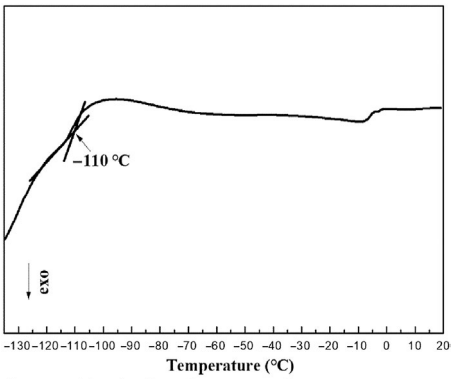

Source(s): Authors' own work

Figure 3. DSC measurement results of the low-phenyl silicone rubber

results indicated that the prepared low-phenyl silicone rubber had excellent low-temperature resistance.

Storage modulus E' serves as an important indicator that can directly reflect rubber elasticity (Zhu, Dai, & Tu, 2017; Zhu *et al.*, 2021). DMA measurements were performed on the prepared low-phenyl silicone rubber in the temperature range of −130 °C–150 °C, and the results were shown in Figure 4. The peak loss factor tanδ was 0.47, and the storage modulus Tg (−105 °C) was slightly higher than the temperature measured during DSC. After the stage of glass transition, the storage modulus dramatically declined, and the rubber entered into a high elastic state, which was consistent with the DSC results. No crystallization transformation was observed, and the sample belonged to non-crystalline rubber, maintaining good elasticity properties under low temperatures.

The thermal stability of sealing ring rubber can directly affect sealing performance and service life. The TGA curve and derivative thermogravimetry (DTG) curves of the prepared low-phenyl silicone rubber are shown in Figure 5, indicating that the sample decomposition process mainly includes two rapid loss stages. Before 200 °C, the low-phenyl silicone rubber generally did not decompose, while between 200 °C and 450 °C, the weight loss slowly decreased, and thermal decomposition started to occur. With increasing temperature, the thermal decomposition rate rapidly increased, the thermal decomposition of molecular chains

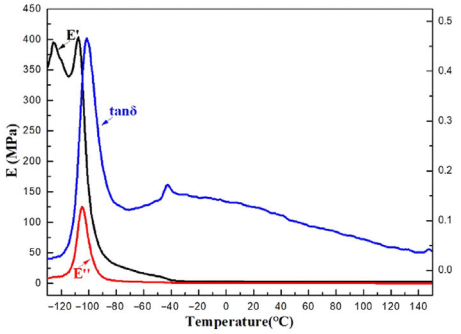

Source(s): Authors' own work

Figure 4. DMA measurement results of the low-phenyl silicone rubber

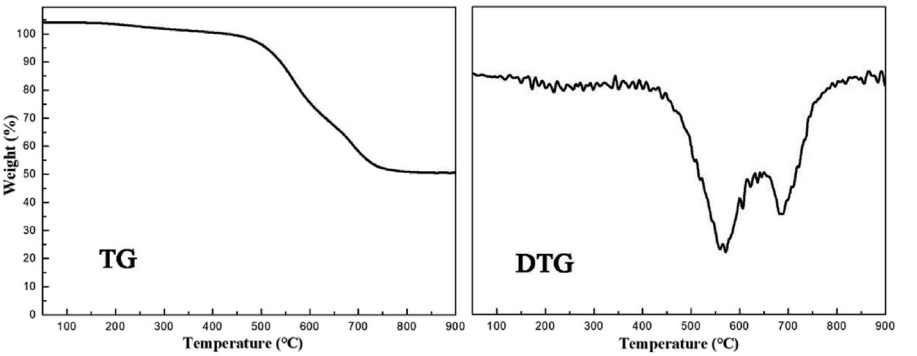

Source(s): Authors' own work

Figure 5. TGA and DTG measurement results of the low-phenyl silicone rubber

dominated, and the sample essentially decomposed at 750 °C, with a final residual amount of about 50%. Before 450 °C, the weight only decreased by about 3.3%, since the recipe for low-phenyl silicone rubber did not contain low-molecular-weight organic additives such as low-temperature plasticizer (Lou *et al.*, 2018; Zhu *et al.*, 2024). This indicated that the low-temperature resistance was well maintained and the low-temperature resistance of other rubber types could quickly decrease as the low-temperature plasticizer in the recipe precipitated under high-temperature conditions or under long-term use. The first stage of thermal decomposition was approximately 450 °C-650 °C, in which some side-chain groups were mainly broken and decomposed, and the highest weight loss rate was reached at approximately 560 °C. The second stage occurred at about 650 °C-750 °C, which involved depolymerization and fracture of the polymer backbone structure, and the highest weight loss rate was reached at about 688 °C. (Huang *et al.*, 2021; Wang *et al.*, 2023, 2024) The Si-O bond on the main chain of the silicone rubber had relatively high bond energy, thus, the thermal stability of silicone rubber was high. The introduction of a small amount of phenyl groups possibly prevented the continued crosslinking or degradation of the main chain caused by the decomposition of side-chain groups, thus, enhancing the thermal stability of this silicone rubber. The above findings indicated that the prepared low-phenyl silicone rubber had excellent thermal stability.

3.2 Finite element analysis of the low-phenyl silicone rubber sealing ring

The O-ring had a circular cross-section, with a simple structure, small size, and easy installation, allowing it to be used in various static and dynamic sealings (Zhou, Zheng, Gu, Zhao, & Liu, 2017). The rectangular sealing ring had a rectangular cross-section, featuring a simple structure, strong anti-extrusion ability, and high sealing pressure, allowing it to be only used for static sealings (Yu, Cui, Zhang, Wang, & Zhong, 2022; Zhang, Wang, Xia, Li, & He, 2016). Static sealing can be used in sealing rings in the flanges of railway freight car brake pipes. According to the requirements in Q/CR 706–2019, sealing performance tests were performed, including conventional assembly (no adjustment gasket) and gap assembly (1.8–0.15 mm adjustment gasket) at both ambient temperature and room temperature (−50 °C), and the depth and width of the flange grooves were only 5.00 and 6.0 mm, respectively. To meet the above experimental requirements, in combination with the advantages of O-rings and rectangular sealing rings, a novel sealing ring was designed in this work, with the structure shown in Figure 1. The modulus parameters of the low-phenyl silicone rubber and Abaqus software were used to conduct the simulation and analysis, with the aim of providing new methods and the means to optimize the design of sealing rings and enhance design accuracy.

3.2.1 Impact of compression ratio and temperature on the stress distribution of sealing ring. Figures 6 and 7 present the Mises stress and contact stress cloud charts of the sealing ring at room temperature and a low temperature of −15 °C when the compression ratio was 15% and the working pressures were 0 and 0.6 MPa, respectively. Through comparison, it could be find that when the working pressure was 0 MPa, the maximum contact stress and maximum Mises stress values of the sealing ring at different temperatures occurred at the same location, and the maximum Mises stress was located at the upper and lower compression points of the sealing ring. In addition, the maximum contact stress was located at the side of the sealing ring close to the flange body. When the working pressure was 0.6 MPa, the maximum Mises stress and maximum contact stress of the sealing ring at different temperatures occurred at different locations. The maximum Mises stress of the room-temperature sample was located where compression occurred between the sealing ring and the outer edge of the groove. The maximum Mises stress of the low-temperature sample occurred at the upper and lower compression points of the sealing ring. The maximum contact stresses of them were located at the side of the sealing ring close to the flange. The contact stress at the area where the room-temperature sample was compressed with the outer edge of the groove was also relatively large. To ensure the sealing effect, the finish of the flange sealing surface and the outer edge of the groove should be improved (Zhou *et al.*, 2014; Zhou & Liu, 2018), with no burrs to avoid extrusion damage to the sealing ring.

Figures 8 and 9 show the Mises stress and contact stress cloud charts of the sealing ring at room temperature and a low temperature of −50 °C when the compression ratio was 37.5%

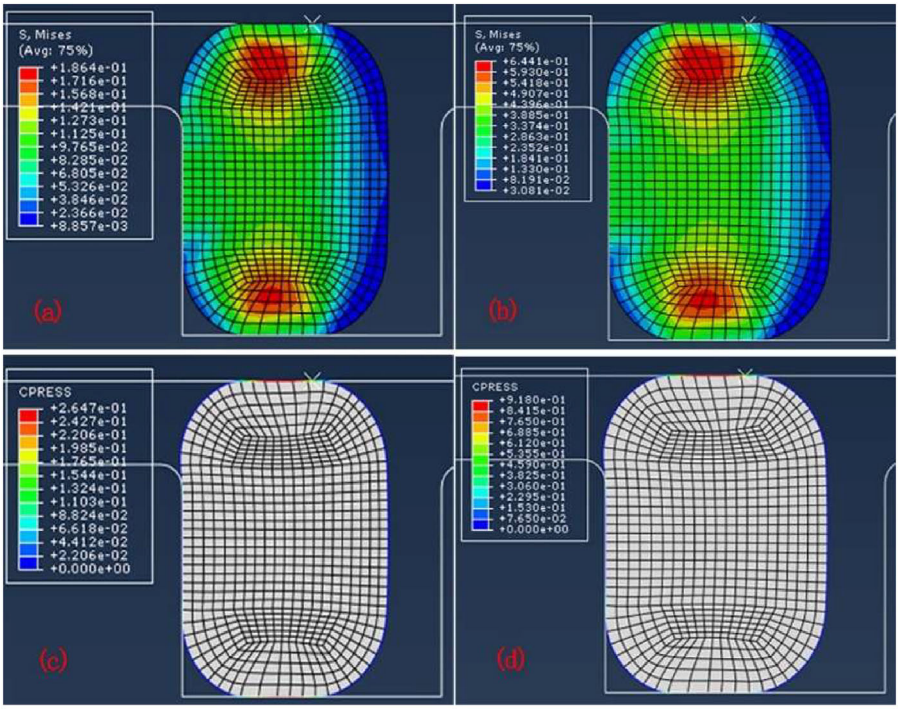

Source(s): Authors' own work

Figure 6. Mises stress and contact stress of a low-phenyl silicone rubber sealing ring at room temperature (a, c) and low temperature −50 °C (b, d) when the compression ratio was 15% (gap of 1.8 mm, sealing air pressure of 0 MPa)

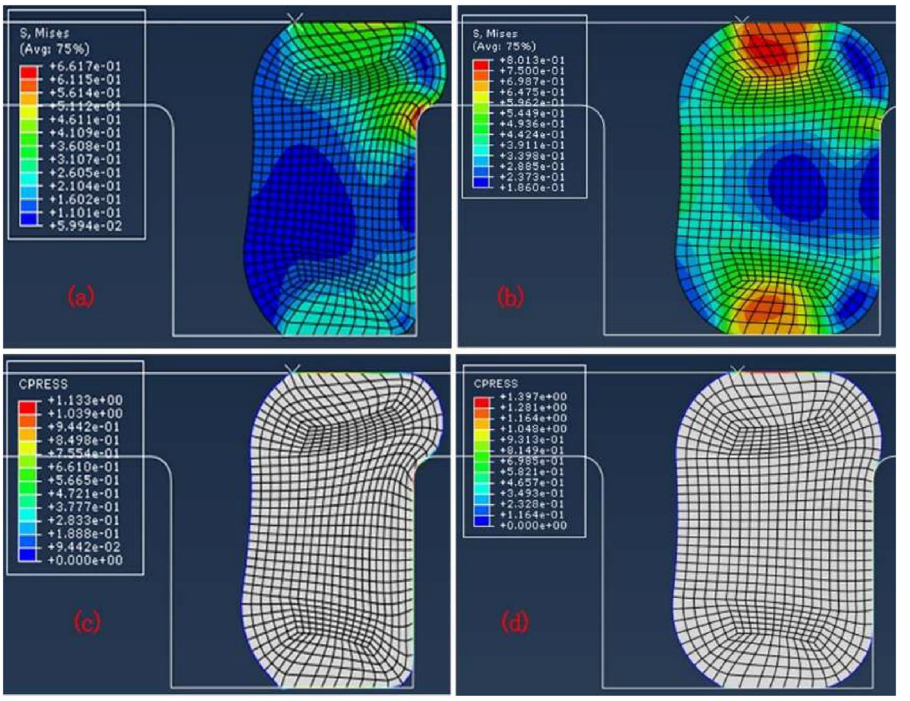

Source(s): Authors' own work

Figure 7. Mises stress and contact stress of the low-phenyl silicone rubber sealing ring at room temperature (a, c) and low temperature of −50 °C (b, d) when the compression ratio was 15% (gap of 1.8 mm, sealing air pressure of 0.6 MPa)

and the working pressures were 0 and 0.6 MPa, respectively. Through comparison, it could be found that when the working pressure was 0 MPa, the maximum Mises stress and maximum contact stress of the sealing ring at different temperatures occurred essentially at the same location. In addition, the maximum Mises stress was located at the compression points of the sealing ring, and the maximum contact stress was located at the side of the sealing ring close to the flange body. When the working pressure was 0.6 MPa, the maximum Mises stress and maximum contact stress of the sealing ring at different temperatures occurred at different locations. The maximum Mises stress of the room-temperature sample occurred at the gap between the flange and outer edge of the groove. The maximum Mises stress of the low-temperature sample extended from its compressed area to the gap between the flange and the outer edge of the groove. The maximum contact stresses of them were all located at the side of the sealing ring close to the flange. To ensure a sealing effect, during sealing ring assembly, extrusion damage to the sealing ring should be avoided at the gap between the flange and outer edge of the groove (Park, Son, Choi, Lee, & Choi, 2023; Tang, He, Zhu, & Zhou, 2019).

3.2.2 Analysis of the maximum contact stress of the low-phenyl silicone rubber sealing ring. Sealing between the sealing ring and flange joint involved a radial seal. According to sealing theory, the necessary and sufficient condition to realize reliable sealing involves contact stress on the continuous interface between the sealing ring and flange body, which should not be less than the working pressure. Table 2 presents a comparison of the maximum contact stress of the sealing surface under different compression ratios and different pressures. According to the table, under the same amount of compression, the contact stresses corresponding to a state with

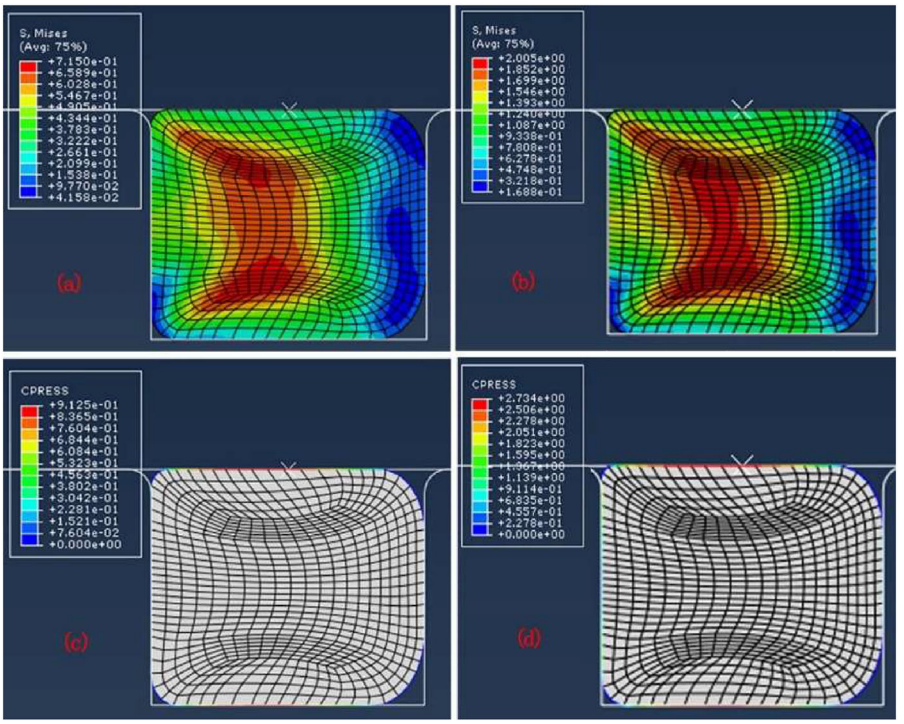

Source(s): Authors' own work

Figure 8. Mises stress and contact stress of the low-phenyl silicone rubber sealing ring at room temperature (a, c) and low temperature of −50 °C (b, d) when the compression ratio was 37.5% (zero-gap seal, sealing air pressure of 0 MPa)

pressure, high compression ratio, and low-temperature state were higher and the values were all higher than the air pressure 0.6 MPa, which met the sealing requirements. Failure leakage only occurred with air pressure, and under high compression ratio and/or low-temperature environments, and the sealing rings were more susceptible to damage (Tang *et al.*, 2019; Zheng *et al.*, 2021). Therefore, provided that sealing was ensured, the selected compression ratio should be as small as possible. To ensure the sealing effect, under a low-temperature working condition, rubber materials with hardness and elasticity less affected by temperature should be used.

3.3 Testing the sealing performance of the low-phenyl silicone rubber sealing ring

A low-phenyl silicone rubber sealing ring (specification DN32) was prepared according to the procedures described in Section 2.4, and its rubber performance parameters are shown in Table 1. According to the experimental requirements of Q/CR 706–2019, at room temperature, the low-phenyl silicone rubber sealing ring was used in the testing fixture shown in Figure 10 (a), and the test device was connected as shown in Figure 10 (b).

The results of testing the sealing performance of the low-phenyl silicone rubber sealing ring are shown in Table 3. Under room temperature and at the low temperature of −50 °C, the leakage amounts in the various sealing performance tests were all zero. During the fracture experiment, fracture did not occur, thus, the prepared low-phenyl silicone rubber sealing ring met the use requirements of flange joints of railway freight car brake pipe systems in the above working conditions in China.

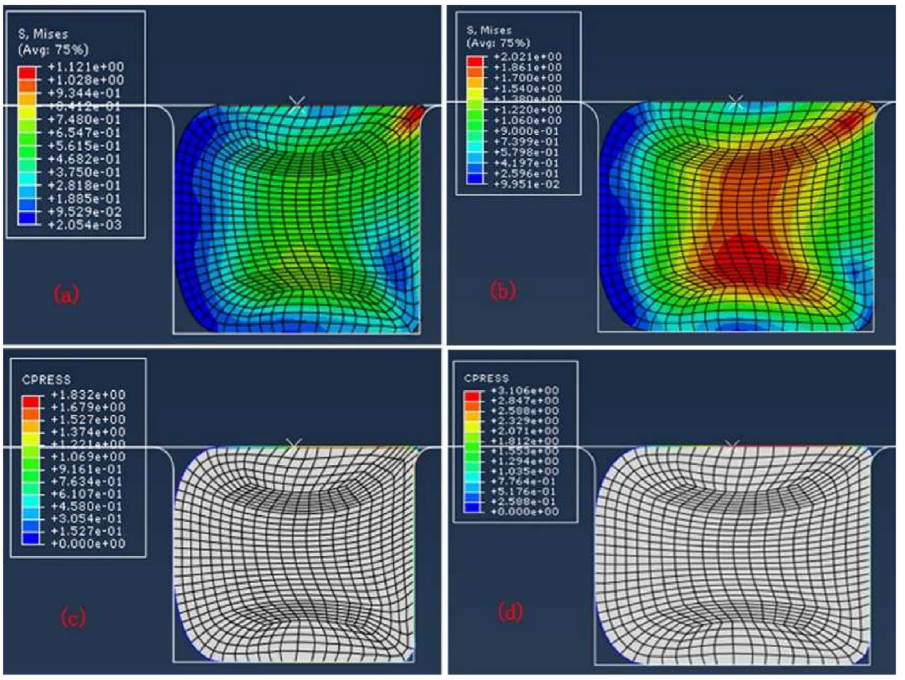

Source(s): Authors' own work

Figure 9. Mises stress and contact stress of the low phenyl silicone rubber sealing ring at room temperature (a, c) and low temperature of −50 °C (b, d) when the compression ratio was 37.5% (zero-gap seal, sealing air pressure of 0.6 MPa)

Table 2. Comparison of the maximum contact stress of the sealing surface at different compression ratios and air pressures

		Maximum contact stress (MPa)			
		Room temperature		Low temperature −50 °C	
No.	Pressure (MPa)	Compression ratio 15%	Compression ratio 37.5%	Compression ratio 15%	Compression ratio 37.5%
1	0	2.647×10^{-1}	9.125×10^{-1}	9.180×10^{-1}	1.832
2	0.6	1.133	2.734	1.397	3.106

Source(s): Authors' own work

4. Conclusions

(1) The modulus at room temperature and the modulus at the low temperature of −50 °C for the prepared low-phenyl silicone rubber sealing ring were very similar. The compression cold-resistance coefficient was 0.73, the measured Tg was −110 °C, the weight loss at 450 °C was only 3.3%, and the sealing ring exhibited excellent low-temperature resistance and thermal stability.

(2) According to the finite element analysis results, to ensure the sealing effect, the finish of the flange sealing surface and the outer edge of the groove should be improved, and extrusion damage to the sealing ring at the gap between the flange body and the outer

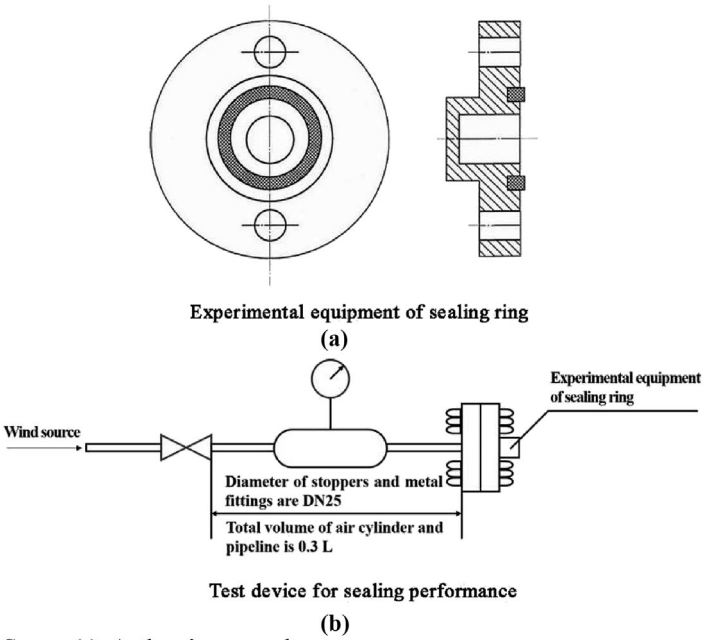

Source(s): Authors' own work

Figure 10. Schematic diagram of the sealing ring testing fixture and sealing performance test device

Table 3. Results of testing the sealing performance of the low-phenyl silicone rubber sealing ring

No.	Test item	Test results	Requirements in Q/CR 706–2019
1	Conventional leakage test at room temperature (kPa/min)	0	≤1
2	Leakage test of the gap assembly at room temperature (kPa/min)	0	≤5
3	Fracture test	No fracture	No fracture
4	Conventional leakage test at low temperature (−50 °C for 24 h) (kPa/min)	0	≤2
5	Leakage test of the gap assembly at low temperature (−50 °C for 24 h) (kPa/min)	0	≤12

Source(s): Authors' own work

edge of the groove should be avoided. Under a high compression ratio and/or low-temperature environment, the sealing ring was more susceptible to damage. Provided that sealing is ensured, the selected compression ratio should be as small as possible. To ensure the sealing effect, under low-temperature working conditions, rubber materials with hardness and elasticity less affected by temperature should be used.

(3) Under room temperature and the low temperature of −50 °C, the leakage amounts of the prepared low-phenyl silicone sealing ring in the results of sealing performance tests were all zero, meeting the use requirements of flange joints of railway freight car brake pipe systems in the above working conditions in China.

References

Akhlaghi, S., Pourrahimi, A. M., Sjöstedt, C., Bellander, M., Hedenqvist, M. S., & Gedde, U. W. (2017). Degradation of fluoroelastomers in rapeseed biodiesel at different oxygen concentrations. *Polymer Degradation and Stability*, *136*, 10–19. doi: 10.1016/j.polymdegradstab.2016.12.006.

Akhtar, M., Qamar, S. Z., Pervez, T., & Al-Jahwari, F. K. (2018). Performance evaluation of swelling elastomer seals. *Journal of Petroleum Science and Engineering*, *165*, 127–135. doi: 10.1016/j.petrol.2018.01.064.

Cheng, G. L., Guo, F., Zang, X. H., Zhang, Z. X., Jia, X. H., & Yan, X. L. (2022). Failure analysis and improvement measures of airplane actuator seals. *Engineering Failure Analysis*, *133*, 105949. doi: 10.1016/j.engfailanal.2021.105949.

Cui, K. B., Qin, J. Q., Di, C. C., & Yang, Y. F. (2014). Finite element analysis and simulation of the sealing performance of Y-ring rubber seal. *Advances in Computational Modeling and Simulation*, *444-445*, 1379–1383. doi: 10.4028/www.scientific.net/amm.0.1379.

Fu, Q. H. (2022). A full-section asphalt concrete waterproof sealing structure for the high-speed railway subgrade. *Railway Sciences*, *1*(2), 193–209. doi: 10.1108/rs-04-2022-0013.

Gao, M., Pan, A. H., Huang, Y., Wang, J. Q., Zhang, Y., Xie, X., . . . Jia, Y. H. (2024). Low-temperature characteristics of rubbers and performance tests of type 120 emergency valve diaphragms. *Railway Sciences*, *3*(1), 47–58. doi: 10.1108/rs-10-2023-0034.

Hu, Y., Zhang, J., & Chen, L. M. (2020). Design and seal performance analysis of bionic sealing ring for dynamic seal. *Mechanika*, *26*(4), 338–345. doi: 10.5755/j01.mech.26.4.23264.

Huang, Y. H., Mu, Q. H., & Su, Z. T. (2021). High and low temperature resistance of phenyl silicone rubber. *IOP Conference Series: Materials Science and Engineering*, *1048*(1). doi: 10.1088/1757-899x/1048/1/012001.

Jing, S., Mu, A. L., Zhou, Y., & Xie, L. (2020). Finite-element analysis and structure optimization of X-O composite seal of cone bit. *Advances in Mechanical Engineering*, *12*(5), 1–12. doi: 10.1177/1687814020918686.

Lee, S. H., Yoo, S. S., Kim, D. E., Kang, B. S., & Kim, H. E. (2012). Accelerated wear test of FKM elastomer for life prediction of seals. *Polymer Testing*, *31*(8), 993–1000. doi: 10.1016/j.polymertesting.2012.07.017.

Li, J. X., Liu, P. F., Wang, S. B., & Leng, J. X. (2020). Finite element analysis of O-ring sealing performance of manned submersible viewports. *Journal of Failure Analysis and Prevention*, *20*(5), 1628–1637. doi: 10.1007/s11668-020-00970-2.

Liu, F. S., Yang, G., Chen, Z. Y., Zhang, Y. H., & Zhou, Q. Y. (2023). Development of rail technology for high speed railway in China. *Railway Sciences*, *2*(4), 431–446. doi: 10.1108/rs-08-2023-0026.

Lou, W. T., Zhang, W. F., Jin, T. Z., Liu, X. R., & Dai, W. (2018). Synergistic effects of multiple environmental factors on degradation of hydrogenated nitrile rubber seals. *Polymers*, *10*(8), 897. doi: 10.3390/polym10080897.

Lv, Y., Yi, S. N., Zhu, L. P., Chen, G. S., & Li, F. P. (2009). Development of E-shaped double-sided active sealing flange seal ring for the braking pipeline system. *Rolling Stock*, *47*(10), 11–14.

Nakanishi, Y., Mita, K., Yamamoto, K., Ichino, K., & Takenaka, M. (2021). Effects of mixing process on spatial distribution and coexistence of sulfur and zinc in vulcanized EPDM rubber. *Polymer*, *218*, 123486. doi: 10.1016/j.polymer.2021.123486.

Park, W. M., Son, S. M., Choi, D. K., Lee, H. G., & Choi, C. (2023). Oil-sealing performance evaluation of labyrinth seal using combined finite element analysis and computational fluid dynamics. *Lubricants*, *11*(9), 400. doi: 10.3390/lubricants11090400.

Song, R. H., Yang, R., Wang, C., & Su, Z. T. (2024). Effects of filler content on non-linear viscoelasticity of high fluorine content fluoroelastomer mixture investigated through large amplitude oscillatory shear tests. *Journal of Rubber Research*, *27*(3), 1–15.

Tang, L. P., He, W., Zhu, X. H., & Zhou, Y. L. (2019). Sealing performance analysis of an end fitting for marine unbonded flexible pipes based on hydraulic-thermal finite element modeling. *Energies*, *12*(11), 2198. doi: 10.3390/en12112198.

Tao, N. N. (2023). Thermodynamic and sealing performance analysis of reciprocating O-rings in hydraulic cylinders. *International Journal of Heat and Technology*, *141*(3), 694–700. doi: 10.18280/ijht.410323.

Wang, S. Q., Peng, Z. B., Huang, Y. H., Zhu, M. Q., Liu, Y. Y., & Zhang, Y. (2024). Synthesis, characterization and properties of vinyl-terminated poly [dimethylsiloxane-co-methyl(phenyl) siloxane]. *Polymer*, *311*, 127554. doi: 10.1016/j.polymer.2024.127554.

Wang, C., Ren, J. X., Liu, Y., Hao, W. Q., & Yang, J. X. (2013). Analysis of silicone rubber elastomer elastic failure in small-size flexible joint at low temperature. *Key Engineering Materials*, *575-576*, 427–433. doi: 10.4028/www.scientific.net/kem.575-576.427.

Wang, X. S., Zhang, Y. B., Ren, S. Y., Xu, Z. H., Li, K. S., Hao, X. X., & He, Q. (2023). Effect of zinc oxide/layered double hydroxide on the mechanics of silicone rubber at low temperature. *European Polymer Journal*, *200*, 112478. doi: 10.1016/j.eurpolymj.2023.112478.

Yu, Y. J., Cui, Y., Zhang, H. X., Wang, D. W., & Zhong, J. J. (2022). Evaluation analysis on leakage performance for beam seal with two sealing areas. *IEEE Access*, *10*, 29916–29924. doi: 10.1109/access.2022.3158485.

Zhang, X., Wang, G., Xia, P., Li, H. P., & He, M. (2016). Finite element analysis and experimental study on contact pressure of hydraulic support bud-shaped composite sealing ring. *Advances in Mechanical Engineering*, *8*(10), 1–9. doi: 10.1177/1687814016674846.

Zheng, C., Zheng, X. F., Qin, J., Liu, P., Aibaibu, A., & Liu, Y. H. (2021). Nonlinear finite element analysis on the sealing performance of rubber packer for hydraulic fracturing. *Journal of Natural Gas Science and Engineering*, *85*, 103711. doi: 10.1016/j.jngse.2020.103711.

Zhou, Y., & Liu, Y. H. (2018). Newly structured design and finite element analysis of bionic nonsmooth surface sealing ring of cone bit. *Advances in Mechanical Engineering*, *10*(3), 617–626. doi: 10.1177/1687814018767704.

Zhou, Y., Huang, Z. Q., Tan, L., Ma, Y. C., Qiu, C. S., Zhang, F. X., ... Guo, L. (2014). Cone bit bearing seal failure analysis based on the finite element analysis. *Engineering Failure Analysis*, *45*, 292–299. doi: 10.1016/j.engfailanal.2014.07.007.

Zhou, C. L., Zheng, I. Y., Gu, C. H., Zhao, Y. Z., & Liu, P. F. (2017). Sealing performance analysis of rubber O-ring in high-pressure gaseous hydrogen based on finite element method. *International Journal of Hydrogen Energy*, *42*(16), 11996–12004. doi: 10.1016/j.ijhydene.2017.03.039.

Zhu, H. J., Dai, Z. L., & Tu, W. P. (2017). Study on the preparation and performance of low gas permeability trifluoropropyl phenyl silicone rubber. *Rsc Advances*, *7*(63), 39739–39747. doi: 10.1039/c7ra07195g.

Zhu, M., Ma, D. S., Zhou, Y., Huang, H. Y., Shao, Z. Q., Wu, F., & Li, B. (2024). The change of sealing property in the aging process of NBR sealing equipment based on finite element analysis. *Coatings*, *14*(9), 1178. doi: 10.3390/coatings14091178.

Zhu, L., Zhao, S. G., Zhang, C., Cheng, X., Hao, J. H., Shao, X. Q., & Zhou, C. J. (2021). Effects of chain structure on damping property and local dynamics of phenyl silicone rubber: Insights from experiment and molecular simulation. *Polymer Testing*, *93*, 106885. doi: 10.1016/j.polymertesting.2020.106885.

Corresponding author
Ming Gao can be contacted at: hebeigm2008@126.com